PERGAMON

International Journal of Heat and Mass Transfer 45 (2002) 3621–3629

International Journal of HEAT and MASS TRANSFER

www.elsevier.com/locate/ijhmt

Heat transfer in pulse-stabilized fluidization – Part 2: local, instantaneous analysis

Deborah V. Pence [a,*], Donald E. Beasley [b]

[a] Department of Mechanical Engineering, Oregon State University, 204 Rogers Hall, Corvallis, OR 97331, USA
[b] Department of Mechanical Engineering, Clemson University, Box 340921 Clemson, SC 29634, USA

Received 19 November 2000; received in revised form 31 January 2002

Abstract

Enhancements in overall heat transfer from a heated, submerged horizontal cylinder in a pulse-stabilized fluidized bed were observed in Part 1 for operating conditions with low primary and secondary flow rates and low pulse frequencies. These increases in overall heat transfer were found to be a consequence of significant localized enhancements. In the present paper, through spectral and contact time analyses of local, instantaneous heat transfer, increases in both bubble phase and emulsion phase heat transfer coefficients were observed. Instantaneous measurements in a monodisperse distribution of 345 μm particles, fluidized to rates from 1.1 to 1.5 times greater than that required for minimum fluidization, are investigated. Waveforms of these time traces are characterized as exhibiting either locally or globally dominated hydrodynamic phenomena. Heat transfer with an opposing oscillatory flow exhibits characteristics of globally dominated hydrodynamics, whereas heat transfer traces acquired near minimum fluidization with no secondary flow are dominated by hydrodynamics localized at the surface of the cylinder.

1. Introduction

In Part 1 of this paper, experimental results describing the effect of an opposing oscillatory flow on overall and local time-averaged heat transfer from a submerged horizontal cylinder to a laboratory-scale bubbling fluidized bed were presented. The state of fluidization created under these conditions is termed "pulse-stabilized fluidization". In Part 2, results documenting the local instantaneous heat transfer in pulse-stabilized fluidization are presented. These time-resolved measurements provide phenomenological insight into the changes in the heat transfer rate created by the altered hydrodynamics in pulse-stabilized fluidization.

Previous studies relevant to the present investigation will be briefly reviewed. These studies used time-resolved measurements of a system variable, such as void fraction or heat flux, to characterize the hydrodynamics or heat transfer. In addition, average emulsion phase contact times have been evaluated for both vertical and horizontal cylinders using several measurement techniques. Ozkaynak and Chen [1] evaluated emulsion phase contact times associated with a vertical cylinder using time-dependent measurements of capacitance. Baskakov et al. [2] determined average emulsion phase contact times using a heat flux probe and developed empirical correlations for estimating bubble fraction and average emulsion phase contact times for vertical cylinders. Pence et al. [3], Mueller et al. [4], and Pence [5] employed experimental data from horizontal heat transfer surfaces to develop heat transfer correlations employing the form proposed by Baskakov et al. [2]. Chandran and Chen [6] determined root-square-average residence times of the emulsion phase using local instantaneous void fraction data acquired with a capacitance probe embedded in a horizontal cylinder, whereas Kurosaki et al. [7] conducted a study of the average particle residence times at the surface of a horizontal cylinder using fiber optic techniques.

* Corresponding author. Tel.: +1-541-737-7018; fax: +1-541-737-2600.
E-mail address: pence@engr.orst.edu (D.V. Pence).

0017-9310/02/$ - see front matter
PII: S0017-9310(02)00068-6

Nomenclature

A_{eff}	effective area of heat flux probe (m^2)
A_s	surface area of horizontal copper cylinder (m^2)
E_b	time-averaged bridge circuit voltage for constant heat flux probe temperature (V)
E_c	potential supplied to cartridge heater (V)
f	forcing frequency of piston (Hz)
$f^y_{x,\theta}$	average fraction of phase y at angular position θ and a flow condition of x
$h_{x,\theta}(t)$	local, instantaneous heat transfer coefficient at angular position θ and flow condition x (W/m^2 K)
h	overall cylinder heat transfer coefficient (W/m^2 K)
h_θ	time-averaged local heat transfer coefficient measured at angular position θ (W/m^2 K)
$h_{x,\theta}$	time-averaged local heat transfer coefficient at angular position θ and flow condition x (W/m^2 K)
$h^y_{x,\theta}$	average heat transfer coefficient of phase y at angular position θ and flow condition x (W/m^2 K)
I_c	current supplied to cartridge heater (A)
Q_{eq}	equivalent flow rate: total flow rate is introduced through plenum (m^3/s)
Q_{mf}	flow rate corresponding to minimum fluidization (m^3/s)
Q_p	primary flow rate, plenum (m^3/s)
Q_s	secondary flow rate, pulse simulator (m^3/s)
Q_t	total flow rate: sum of primary and secondary flow rate (m^3/s)
r	driving link radius for pulsed flow simulator (mm)
R_b	bridge circuit resistance (10 Ω)
R_c	cable resistance (Ω)
R_p	probe resistance (Ω)
t	time (s)
T_b	average temperature of fluidized bed media (°C)
T_p	probe temperature (°C)
T_s	surface temperature of horizontal copper cylinder (°C)
V_k	kinematic velocity amplitude at exit of pulsed flow simulator tailpipe (m/s)
V_r	resonant velocity amplitude at exit of pulsed flow simulator tailpipe (m/s)

Greek symbols

γ	power spectral density (W^2/m^4 K^2 Hz)
v	frequency (Hz)
θ	angular position around horizontal cylinder: measured from stagnation point (degrees)

Superscripts (phase – y)

b	bubble phase
s	steady-state heat transfer resulting from mixing emulsion phase contact
t	transient heat transfer resulting from stationary emulsion phase contact

Subscripts (operating condition – x)

eq	equivalent flow condition, total flow through plenum only
f	forcing frequency of secondary stream ($f = 0, 5, 10, 15$ Hz)
p	primary flow condition

Several studies suggest two distinct types of emulsion phase contact at a surface for bubbling fluidization. Kurosaki et al. [8] employed fiber optics to observe particle behavior at a submerged surface, and observed that particles may be either stationary or in motion during emulsion phase contact with the surface. George [9] identified two distinct types of emulsion phase contacts in a high temperature fluidized bed from time resolved measurements, but did not quantify the contact times associated with the emulsion phase contact dynamics. Pence et al. [3] distinguished between and quantified the average contact times for two distinct types of emulsion phase behavior associated with heat transfer to a submerged surface. The first type of emulsion phase contact results from the emulsion phase forming a close-packed geometry at the surface, resulting in transient decay of the heat transfer rate. The second type of emulsion phase contact involves local particle motion in the vicinity of the surface, resulting in a heat transfer coefficient that fluctuates about an average value, rather than decays with time.

Several studies have reported methods for altering the hydrodynamics in bubbling fluidized beds with the goal of improving transport rates. Kobayashi et al. [10,11] experimentally investigated the effects of pulsing the fluidizing air flow upstream of the distributor, whereas Nowak et al. [12] subjected a bed to a downward-facing acoustic field from a speaker. Yates et al. [13], Shen et al. [14], and Ding and Gidaspow [15] each employed a secondary gas stream submerged in the bed in opposition to the plenum air stream. However, none of these studies reported local, instantaneous heat transfer coefficients or contact dynamics. For the present work, an opposing oscillatory flow was superimposed on a steady secondary flow, and local instantaneous heat transfer rates were measured. The heat transfer results

are discussed with respect to the corresponding local and global hydrodynamics for various operating conditions.

2. Experimental facility

A Pulsed Atmospheric Fluidized Bed Combustor (PAFBC) is a hybrid combustor that couples a pulsed combustor with an atmospheric bubbling fluidized bed and provides technical advantages in energy efficiency and emissions. A primary fluidization flow through a traditional distributor at the bottom of the fluidized bed and an opposing downward flow having an oscillatory component from the pulsed combustor create the fluidization conditions in a PAFBC. A laboratory-scale experimental facility, shown in Fig. 2 of Part 1 of this paper, was designed and instrumented to examine the effects of a secondary flow rate and frequency and amplitude of an oscillating opposing flow on pressure drop and heat transfer in a gas-fluidized bed.

Details of the experimental facility are provided in Part 1 of this paper and briefly summarized in the present paper (Part 2). The test section had a cross-sectional flow area of 0.305 m × 0.305 m and a height of 0.53 m. The fluidized particulate, spherical glass beads having a narrow size distribution (monodisperse) with a weight mean diameter of 345 μm and a density of 2.5 g/cm^3, filled the bed to a slumped depth of 0.305 m. Air was used as the fluidizing medium for both the primary and secondary streams.

The oscillating secondary flow field was created by a pulsed flow simulator, shown schematically in Fig. 3 of Part 1 of this paper, that consisted of a steady flow inlet, a reciprocating piston sealed with a rolling diaphragm, and a tailpipe assembly. A model was developed from measured amplitudes at the tailpipe exit, which allowed prediction of the resonant amplitude and agreed to within 5% of measured amplitudes. Table 1 in Part 1 of this paper shows the kinematic velocity amplitude based on the piston displacement and continuity, and the velocity amplitude computed from the resonance model for a given driving link radius and driving frequency of the piston.

Two 3.8 cm horizontal cylinders were positioned 15.25 cm above the distributor plate, one of which was copper and instrumented with a TSI model 1471 platinum film heat flux probe. The copper cylinder was internally heated to a temperature approximately 35 °C above the average bed temperature while the probe, for stability considerations, was maintained at 0.75 °C above the surface temperature of the cylinder using an anemometer bridge circuit. The cylinder and probe were heated and allowed to reach a steady-state condition for steady or steady-periodic operating conditions for the fluidized bed and the pulsed-flow simulator. Variations in bridge voltage with time, required to maintain a constant probe temperature, were recorded for 33 s at a sampling frequency of 500 Hz.

Conversion of the bridge voltage variations to instantaneous heat transfer coefficients was accomplished using an in situ calibration that employed the effective area of the heat flux probe as the calibration constant. The effective area, A_{eff}, was determined by forcing the area-weighted average of the time-averaged local heat transfer coefficients, h_θ, equal to the overall heat transfer coefficient, h. The following three equations illustrate the procedure:

$$h = \frac{E_{\mathrm{c}} I_{\mathrm{c}}}{A_{\mathrm{s}}(T_{\mathrm{s}} - T_{\mathrm{b}})} \tag{1}$$

and

$$h = \frac{\sum_{\theta=0}^{315} h_\theta}{8}, \tag{2}$$

where h_θ was measured at 45° increments and is defined by

$$h_\theta = \frac{E_{\mathrm{b}}^2 R_{\mathrm{p}}}{\left(R_{\mathrm{p}} + R_{\mathrm{b}} + R_{\mathrm{c}}\right)^2 A_{\mathrm{eff}}(T_{\mathrm{p}} - T_{\mathrm{b}})}. \tag{3}$$

Further descriptions of the characteristics of film probes employed for heat flux measurement and the in situ calibration process are found in [16–18].

3. Results

In Part 1, significant enhancements in overall heat transfer coefficients were observed with the introduction of an oscillating, opposing secondary flow in a bubbling gas-fluidized bed of 345 μm particles. The greatest enhancement was observed for a primary fluidization ratio of 1.1, a secondary flow equal to 35% of the primary flow, and a 5 Hz forcing frequency. An increase in overall heat transfer on the order of 12% was observed relative to the heat transfer with the same primary and secondary flow rates but no forcing frequency, which in the present context is referred to as a steady secondary flow. Investigation of time-averaged local heat transfer coefficients revealed that significant enhancement at specific azimuthal positions around the circumference of the cylinder was responsible for the observed enhancement in overall heat transfer.

In this present study, the effects of a steady secondary flow and a secondary flow with an oscillating component on contact dynamics and their influence on local, time-averaged heat transfer rates are investigated. Essential to the interpretation of the results is a clear understanding of the several ways in which air flows into the fluidized bed during pulse-stabilized fluidization, termed here the distribution of flow. In the present context, distribution of the flow represents a concept of proportioning a total flow rate between the primary and secondary streams.

Also, note that the term *primary flow* refers to air that entered the facility through the plenum chamber and the distributor plate. The *secondary flow* entered the facility through the tailpipe of the pulsed flow simulator, and was either steady or had a superimposed oscillatory waveform.

The effects of changes in the total flow rate through the bed, the distribution of the flow between the two opposing streams, and the pulse frequency on local instantaneous heat transfer coefficients are identified through carefully derived normalization methods, as described in Part 1 of this paper.

In the figures to follow, the side of the cylinder corresponding to the angular position of +90° is closest to the pulsed flow simulator tailpipe, and superficial fluidization velocities are normalized by the minimum fluidization velocity of 0.086 m/s ±3%.

Time-averaged local heat transfer coefficients from Part 1 of this paper are shown in Fig. 1 and Table 1 for a primary fluidization ratio, Q_p/Q_{mf}, of 1.1. The data are limited to those angular positions that consistently exhibited surface renewal: ±90°, ±45°, and 0°. Compared with local heat transfer values measured with a primary flow only, $h_{p,\theta}$, increases in the primary flow rate and the introduction of a steady secondary flow resulted in significant localized enhancements in heat transfer, as shown by $h_{eq,\theta}$ and $h_{0,\theta}$, respectively. Increases in the primary flow resulted in enhancements on the order of 75% and 30% for the angular positions of 0° and +45°, respectively. Introduction of the steady secondary flow resulted in increases of 30% at both angular locations. In both cases, there was an increase in the total rate of flow through the bed. Also observed in Fig. 1 is an asymmetry introduced with the steady secondary flow. This asymmetry is also identified for the bubble fraction (Eq. (4)), and average bubble and emulsion phase heat transfer coefficients.

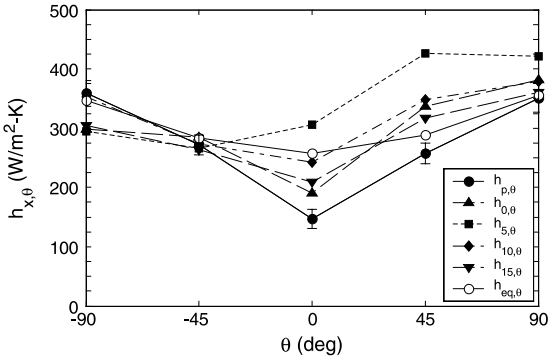

Fig. 1. Time-averaged local heat transfer coefficients ($Q_p/Q_{mf} = 1.1$, $Q_t/Q_{mf} = 1.5$, $Q_s/Q_p = 0.35$).

With a 5 Hz forcing frequency superimposed on the mean secondary flow, enhancements in heat transfer at the stagnation point were on the order of 110%, 20%, and 60% relative to the heat transfer for the primary, equivalent, and steady secondary flow conditions, respectively. Enhancements of approximately 65%, 45%, and 25% were observed at +45°, and 20%, 20%, and 10% at +90° when compared for the same operating conditions, respectively. Less significant enhancements were observed for a 10 Hz forcing frequency, at the same angular positions, and minimal changes were observed for a 15 Hz forcing frequency.

A comparison of $h_{0,\theta}$ with $h_{eq,\theta}$ (Fig. 1) provides an indication of the effect of the flow distribution, for conditions where the total flow rate through the bed is identical. The influence of the pulsing characteristics can be assessed by comparing the heat transfer with a pulsed secondary flow, $h_{f,\theta}$, to that of the steady secondary flow, $h_{0,\theta}$. The typical uncertainty in time-averaged local heat transfer is 6%.

According to Pence et al. [3], time-averaged local heat transfer can be described by:

$$h_{x,\theta} = f^{b}_{x,\theta} h^{b}_{x,\theta} + f^{t}_{x,\theta} h^{t}_{x,\theta} + f^{s}_{x,\theta} h^{s}_{x,\theta}, \quad (4)$$

where the variables f and h on the right-hand side of the equation refer to the fraction of time occupied by and average heat transfer associated with a particular phase, respectively. Superscripts represent the phase, and the

Table 1
Time-averaged local heat transfer coefficients ($Q_p/Q_{mf} = 1.1$, $Q_t/Q_{mf} = 1.5$, $Q_s/Q_p = 0.35$)

	Primary flow condition $h_{p,\theta}$	Steady secondary flow $h_{0,\theta}$	5 Hz combined flow $h_{5,\theta}$	10 Hz combined flow $h_{10,\theta}$	15 Hz combined flow $h_{15,\theta}$	Equivalent flow condition $h_{eq,\theta}$
Q_p/Q_{mf}	1.1	1.1	1.1	1.1	1.1	1.5
Q_t/Q_{mf}	1.1	1.5	1.5	1.5	1.5	1.5
	f (Hz)					
θ (degrees)	N/A	0	5	10	15	N/A
−90	359	298	295	353	305	347
−45	272	285	266	274	264	283
0	147	190	306	242	209	258
+45	258	337	426	348	317	289
+90	351	382	421	379	361	356

first and second subscripts represent the flow conditions and angular position, respectively.

Contact dynamics were extensively examined at the angular positions associated with the lower half of the cylinder as a function of flow rate, flow distribution, and pulsing characteristics for a specific range of operating conditions. Emulsion phase contact was distinguished from bubble phase contact by a dramatic increase in the heat transfer coefficient, on the order 100 W/m^2 K or more, within a period of 10 ms or less. Characterization of emulsion phase as either stationary or mixing in nature was based on the trend in heat transfer during a contact. Further details of the signal analysis procedures are provided in [3,5]. Uncertainties in average values of bubble phase, stationary emulsion phase, and transient emulsion phase heat transfer coefficients are on the order of 7%.

Bubble fraction will be examined as an indicator for changes in the local fluidization hydrodynamics in pulse-stabilized fluidization. Fig. 2 represents the average bubble fraction as a function of angular position for primary flow, equivalent flow, and combined flow conditions with 0, 5, 10, and 15 Hz pulse frequencies in the secondary flow. Consider first the effect of increasing the primary flow rate. At each angular position, increases in bubble fraction resulted from increasing the primary fluidization ratio from 1.1 to 1.5, as shown by $f^{b}_{p,\theta}$ and $f^{b}_{eq,\theta}$, respectively. Because the bubble phase heat transfer is less than that of the emulsion phase, Eq. (4) shows that an increase in bubble fraction results in a decrease in average local heat transfer. Therefore, it is obvious that changes in the bubble fraction did not contribute to the dramatic increase in $h_{eq,\theta}$ relative to $h_{p,\theta}$ at the stagnation point as observed from Fig. 1 and Table 1. However, decreases in bubble fraction resulting from the introduction of a steady or pulsed secondary flow may have contributed to observed increases in heat transfer associated with pulse-stabilization. At the 45° location, the 5 Hz data show the lowest value of bubble fraction, and the largest value of the heat transfer coefficient. Variations in bubble fraction were also observed at −45° where time-averaged local heat transfer coefficients remain essentially constant, regardless of the operating conditions. The typical uncertainty in reported bubble fraction is 7%. These results show that the hydrodynamics of fluidization are significantly affected by the oscillatory secondary flow.

Recall that two distinct types of emulsion phase contacts occur during bubbling fluidization, stationary and mixing, resulting in transient and steady heat transfer, respectively (see Eq. (4)). A comparison of Fig. 3 with Fig. 1 shows that the trends in transient emulsion phase heat transfer coefficients, resulting from stationary emulsion phase contacts, are extremely similar in nature to the trend for time-averaged local heat transfer coefficients. Average steady-state emulsion phase and bubble phase heat transfer coefficients, as a function of angular position and operating conditions, were also remarkably similar to those reported in Fig. 3. In general, average steady-state emulsion phase heat transfer coefficients were within 10% of the average transient emulsion phase heat transfer. This similarity in trends for bubble and emulsion phase heat transfer suggests that the observed increases in heat transfer may be related to a decrease in void fraction in both the lean and dense phases. The results of previous studies that address local void fraction will be discussed.

In general, the average heat transfer coefficients of the emulsion phase (Fig. 3) and bubble phases [5] are observed to increase with angular position and with flow rate, particularly at the stagnation point. In a two-dimensional gas-fluidized bed, Suarez [19] visualized the flow around the lower half of a horizontal cylinder and reported a thin film layer, similar to that observed by Glass and Harrison [20], resulting from local bubble formation. Both Suarez [19] and Glass and Harrison [20] report a decrease in the film thickness with increasing

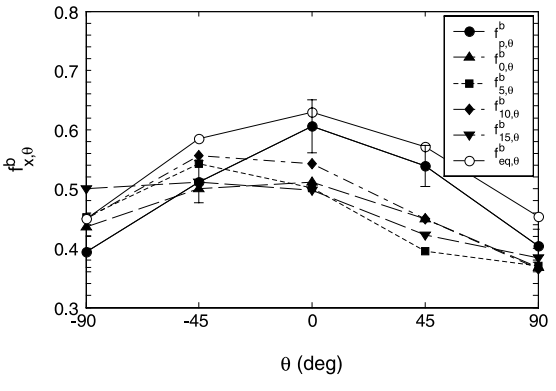

Fig. 2. Average bubble fraction ($Q_p/Q_{mf} = 1.1$, $Q_t/Q_{mf} = 1.5$, $Q_s/Q_p = 0.35$).

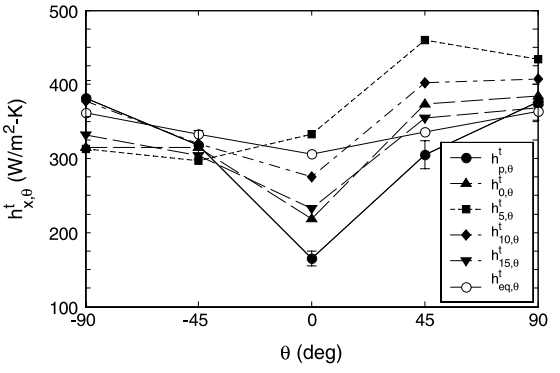

Fig. 3. Average transient (stationary) emulsion phase heat transfer coefficient ($Q_p/Q_{mf} = 1.1$, $Q_t/Q_{mf} = 1.5$, $Q_s/Q_p = 0.35$).

angular position from the stagnation point. Fakhimi and Harrison [21] measured time-averaged void fraction and also report a decrease with increasing angular position. It was also reported in Fakhimi and Harrison [21] that increases in time-averaged void fraction occurred with increases in the flow rate, with the most dramatic differences observed at the stagnation point. Being time-averaged values of void fraction, the observed increase could be a result of increased bubble fraction with increasing flow rate, as was observed in Fig. 2. These two-dimensional investigations provide results that tend to lend support to the idea that increases in heat transfer in pulse-stabilized fluidization may result from decreases in the bubble and emulsion phase void fraction.

Chandran [22] distinguished between the void fraction in the dense phase and the lean phase for a 29 mm diameter horizontal cylinder in a 0.305 m square cross-section fluidized bed, over a range of conditions from incipient fluidization to slugging. Reported trends in bubble fraction and root-square-average residence times of the dense phase as a function of angular position and flow rate for 245 μm particles below the slugging regime are quite similar to the bubble fraction and emulsion phase contact times reported for 345 μm particles in the present study. Average values of lean and dense phase void fractions as a function of angular position and flow rate were also provided by Chandran [22] for 245 μm particles at atmospheric pressure. Below slugging conditions, increases in primary flow rate yielded a trend of decreasing dense and lean phase void fraction at the stagnation point. At the 90° location, the void fraction remains essentially constant with fluidizing velocity, and the dense phase void fraction is significantly lower than at the stagnation point.

Based on the above discussion of previous measurements of void fraction, and the observed changes in heat transfer in pulse-stabilized fluidization, it a reasonable to conclude that it is likely that bubble and emulsion phase void fractions change in pulse-stabilized fluidization, and that these changes in the present system are most likely a result of changes in both the global and local hydrodynamics. Additional insight may be gained by examining the instantaneous heat flux signals.

Because of the significant enhancement in heat transfer at the stagnation point, further examination of the heat transfer at this location was undertaken. Figs. 4(a) and 5(a) show instantaneous heat transfer signals measured at the stagnation point with primary fluidization ratios of 1.1 and 1.5, respectively, and no secondary flow. Chandran and Chen [6] reported sporadic emulsion phase contacts at the stagnation point for low fluidization velocities, and an increase in the frequency of emulsion phase contacts resulting from increases in the plenum flow rate. The same behavior is identified from a comparison of the signals in Figs. 4(a) and 5(a), which

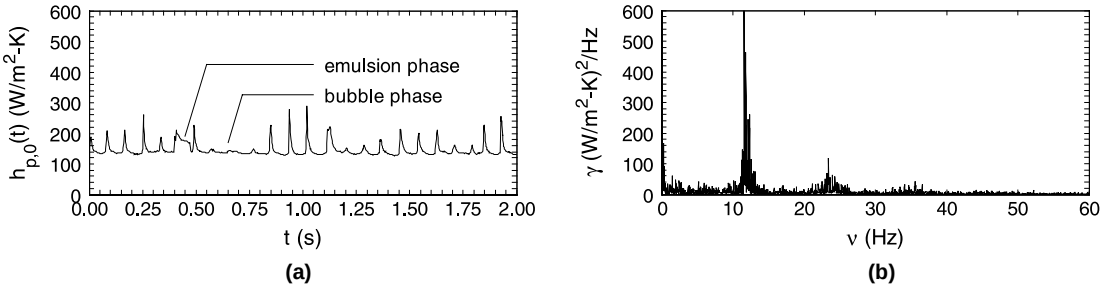

Fig. 4. (a) Local instantaneous heat transfer coefficient, and (b) power spectrum ($\theta = 0,\ Q_p/Q_{mf} = 1.1,\ Q_t/Q_{mf} = 1.1,\ Q_s/Q_p = 0.0$).

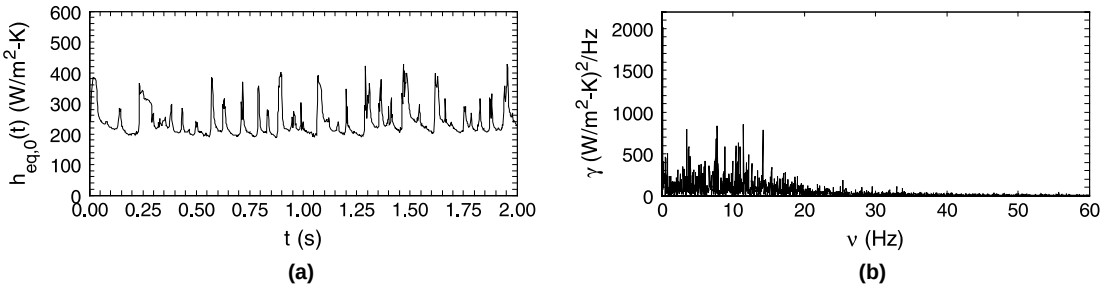

Fig. 5. (a) Local instantaneous heat transfer coefficient, and (b) power spectrum ($\theta = 0,\ Q_p/Q_{mf} = Q_{eq}/Q_{mf} = 1.5,\ Q_t/Q_{mf} = 1.5,\ Q_s/Q_p = 0.0$).

also shows an increase in both average bubble phase and emulsion phase heat transfer coefficients with an increase in primary flow rate.

Power spectra, normalized according to Parseval's theorem, for the signals in Figs. 4(a) and 5(a), less their mean values, are shown in Figs. 4(b) and 5(b), respectively. The natural frequency of the present fluidized bed is very close to 1.8 Hz. Hydrodynamics associated with this natural frequency are *global* in nature. Therefore, the 12 Hz fundamental frequency and the 24 and 36 Hz harmonic frequencies observed in the power spectrum in Fig. 4(b) are believed to be related to local bubble formation. Local bubble formation at the lower half of a submerged horizontal cylinder, referred to as *local* hydrodynamics in the present context, is well documented in the two-dimensional investigations of Ginoux et al. [23], Suarez [19] and Glass and Harrison [20]. Evident from the power spectrum in Fig. 5(b), the energy content exists over a broader range of frequencies than in Fig. 4(b), including peaks near 1.8 and 12 Hz, which suggests an increased contribution of global hydrodynamics and particle mixing during the emulsion phase.

Two seconds of a time-varying heat transfer coefficient, recorded at the stagnation point for a steady secondary flow are shown in Fig. 6(a). Both the bubble phase and emulsion phase heat transfer coefficients are higher than those reported prior to introduction of the secondary flow (Fig. 4(a)). However, the heat transfer coefficients of both phases are lower than those reported for the equivalent flow condition shown in Fig. 5(a), in which the primary fluidization ratio was 1.5. The induced flow pattern by the secondary flow is anticipated to be responsible for this observation.

The *psd* for the signal in Fig. 6(a) is shown in Fig. 6(b). A comparison of Fig. 6(a) with Fig. 4(a) reveals an increase in particle mixing in the emulsion phase with introduction of the secondary flow hydrodynamics and a simultaneous increase in the total flow rate through the bed. The frequency content in Fig. 6(b) is broad-band in nature. When operated with a primary flow near minimum fluidization, changes in the local and global hydrodynamics introduced by a secondary stream resulted in an increase in the broad-band nature of the power spectra, which is evident from a comparison of Fig. 6(b) with Fig. 4(b). These changes are a result of an increase in bubble and emulsion phase contact times, and hence less frequent occurrences of these two phases resulting in a shift in power to lower frequencies.

Comparing Fig. 7(a) with Fig. 6(a), it is evident that superposition of a 5 Hz forcing frequency resulted in longer emulsion phase contact times and higher bubble phase and emulsion phase heat transfer coefficients than those compared with a steady secondary flow. The corresponding power spectrum for the instantaneous

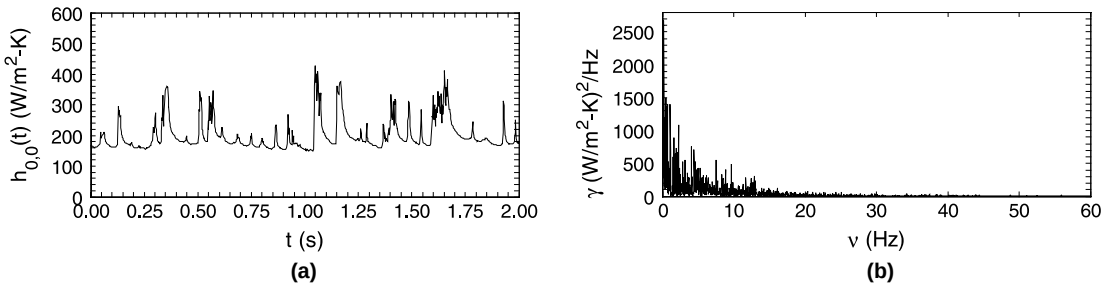

Fig. 6. (a) Local instantaneous heat transfer coefficient, and (b) power spectrum ($\theta = 0,\ Q_p/Q_{mf} = 1.1,\ Q_t/Q_{mf} = 1.5,\ Q_s/Q_p = 0.35,\ f = 0$ Hz).

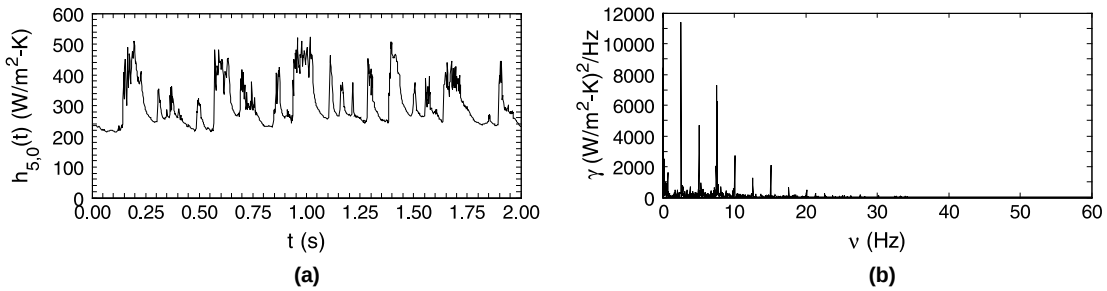

Fig. 7. (a) Local instantaneous heat transfer coefficient, and (b) power spectrum ($\theta = 0,\ Q_p/Q_{mf} = 1.1,\ Q_t/Q_{mf} = 1.5,\ Q_s/Q_p = 0.35,\ f = 5$ Hz).

signal in Fig. 7(a) is shown in Fig 7(b). A fundamental frequency of 2.5 Hz, corresponding to half the forcing frequency of 5 Hz, is observed as well as several harmonics. The 2.5 Hz component is expected to be a result of the large scale or bulk motion of the bed, perhaps the coalescence of bubbles. Such sub-harmonics are possible only in nonlinear systems. Decreases in both the average emulsion phase and bubble phase heat transfer coefficients were observed by Pence [5] at 0°, +45°, and +90° with forcing frequencies of 10 and 15 Hz relative to the heat transfer observed with a 5 Hz forcing frequency. For all forcing frequencies, the local hydrodynamics appear to have been suppressed relative to the global hydrodynamics.

Enhancements in local heat transfer, primarily a result of increases in both the bubble phase and emulsion phase heat transfer, also appear to be related to the waveform characteristics of the instantaneous signal. Signals dominated by local phenomena, such as local bubble formation identified in Fig. 4(a), exhibit sharply peaked emulsion phase heat transfer occurrences, and tend to exhibit lower heat transfer coefficients than signals dominated by global hydrodynamics. The latter signals also tend to have longer emulsion phase contact times, such as those observed in Fig. 5(a).

Heat transfer observed under conditions of secondary flows with a superimposed waveform exhibit characteristics of globally dominated hydrodynamics (Fig. 7(a)). The power spectrum shown in Fig. 7(b) shows that for these operating conditions, the heat transfer phenomena was dominated by global hydrodynamics, and that the natural frequency of the bed was suppressed. The surface renewal occurred at the forcing frequency and its harmonics. Heat transfer for forcing frequencies of 10 and 15 Hz was also dominated by global phenomena, but were lower in value than for a forcing frequency of 5 Hz. Power spectra of the signals acquired with an imposed 10 and 15 Hz forcing frequency did not exhibit sub-harmonics of the forcing frequency. The increase in forcing frequency resulted in a decrease in emulsion phase and bubble phase contact times and a tendency for the waveform to become more sharply peaked during emulsion phase contacts.

4. Conclusions

In Part 1, increases in overall cylinder heat transfer coefficients resulting from the introduction of an oscillating, opposing secondary flow in a bubbling gas-fluidized bed were determined to be the result of local variations. An increase in total flow and the hydrodynamics created by an opposing stream contributed to these heat transfer trends. In the present paper, enhancement in heat transfer resulting from the introduction of a secondary flow, both steady and oscillating, was experimentally investigated through analysis of the local contact dynamics and spectral analysis.

Increases in both the bubble phase and emulsion phase heat transfer coefficients were determined to be the major contributors to observed enhancement in time-averaged local heat transfer, which may be a result of reductions in local void fraction of the lean and dense phases. In addition, characteristic shapes of the instantaneous signals were found to be related to heat transfer trends. Local bubble formation was found to dominate the stagnation point at low flow rates and may have resulted in increased local void fraction of one or both phases. Waveforms of the locally dominated signals were characterized by narrow peaks and low bubble and emulsion phase heat transfer coefficients. Signals dominated by global phenomena generally had longer emulsion phase contacts and higher heat transfer rates than locally dominated signals. The greatest observed enhancement resulted from forcing the secondary flow at 5 Hz, the closest operating frequency to the 1.8 Hz natural frequency of the bed and the only forcing frequency to yield sub-harmonics in the power spectra.

Acknowledgements

Support for this research from Manufacturing Technology Conversion International (MTCI), Thermochem and the Morgantown Energy Technology Center through the South Carolina Institute for Energy Studies is gratefully acknowledged. The PAFBC technology was developed by MTCI and licensed to ThermoChem with support from the US Department of Energy. The contributions of Dr. Momtez Mansour to the conceptual development and implementation of the PAFBC made this research possible. Dr. John Riester contributed significantly to the design of the present experimental facility, and the assistance of M. Cory Postle in the laboratory was invaluable. Special thanks are also extended to Kent Enfield for his assistance with the figures.

References

[1] T.F. Ozkaynak, J.C. Chen, Average residence times of emulsion and void phases at the surface of heat transfer tubes in fluidized beds, AIChE Symp. Series 74 (174) (1978) 334–343.

[2] A.P. Baskakov, B.V. Berg, O.K. Vitt, N.F. Filippovsky, V.A. Kirakosyan, J.M. Goldobin, V.K. Makaev, Heat transfer to objects immersed in fluidized beds, Powder Technol. 8 (1973) 273–282.

[3] D.V. Pence, D.E. Beasley, R.S. Figliola, Heat transfer and surface renewal dynamics in gas fluidized beds, J. Heat Transfer 116 (4) (1994) 929–937.

[4] B.T. Mueller, D.V. Pence, D.E. Beasley, Emulsion phase contact dynamics and heat transfer in large and small particle gas-fluidized beds, in: Proceedings of the ASME/JSME Thermal Engineering Joint Conference, Maui, HI, 1995, pp. 499–508.
[5] D.V. Pence, Studies of heat transfer and chaos in a gas-fluidized bed with an opposing oscillatory flow, Ph.D. Dissertation, Clemson University, Clemson, SC, 1995.
[6] R. Chandran, J.C. Chen, Bed-surface contact dynamics for horizontal tubes in fluidized beds, AIChE J. 28 (6) (1982) 907–914.
[7] Y. Kurosaki, I. Satoh, T. Ishize, Mechanisms of heat transfer enhancement of gas-solid fluidized bed: estimation of direct contact heat exchange from heat transfer surface to fluidized particles using an optical visualization technique, J. Heat Transfer 117 (1995) 104–112.
[8] Y. Kurosaki, H. Ishiguro, K. Takahashi, Fluidization and heat-transfer characteristics around a horizontal heated circular cylinder immersed in a gas fluidized bed, Int. J. Heat Mass Transfer 31 (2) (1988) 349–358.
[9] A.H. George, Instantaneous local heat transfer coefficients and related frequency spectra for a horizontal cylinder in a high temperature fluidized bed, Int. J. Heat Mass Transfer 36 (2) (1993) 337–345.
[10] M. Kobayashi, D. Ramiswami, W.T. Brazelton, Heat transfer from an internal surface to a pulsed bed, Chem. Eng. Progress Symp. Series 66 (105) (1970) 58–67.
[11] M. Kobayashi, D. Ramiswami, W.T. Brazelton, Pulsed-bed approach to fluidization, Chem. Eng. Progress Symp. Series 66 (105) (1970) 4757.
[12] W. Nowak, M. Hasatani, M. Derczynski, Fluidization and heat transfer of fine particles in an acoustic field, AIChE Symp. Series 89 (296) (1993) 137–149.
[13] J.G. Yates, S.S. Cobbinah, D.J. Cheesman, S.P. Jordan, Particle attrition in fluidized beds containing opposing jets, AIChE Symp. Series 87 (281) (1991) 13–19.
[14] Z. Shen, C.L. Briens, M. Kwauk, M.A. Bergougnow, Study of a downward gas jet in a two-dimensional fluidized bed, Can. J. Chem. Eng. 68 (1990) 534–540.
[15] J. Ding, D. Gidaspow, A semi-empirical model for fluidization of fine particles, Ind. Chem. Eng. 36 (4) (1994) 139–150.
[16] D.E. Beasley, R.S. Figliola, A generalised analysis of a local heat flux probe, J. Phys. E 21 (1988) 316–322.
[17] R.S. Figliola, M. Swaminathan, D.E. Beasley, A study of the dynamic response of a local heat flux probe, Measurement Sci. Technol. 4 (1993) 1052–1057.
[18] C. Dinu, D.E. Beasley, R.S. Figliola, Frequency response characteristics of an active heat flux gage, J. Heat Transfer 120 (3) (1998) 577–581.
[19] E. Suarez, Instantaneous, azimuthal and average heat transfer coefficients for a horizontal cylinder submerged in a mixed particle size, gas fluidized bed, Ph.D. Dissertation, Clemson University, Clemson, SC, 1983.
[20] D.H. Glass, D. Harrison, Flow patterns near a solid obstacle in a fluidized bed, Chem. Eng. Sci. 19 (1964) 1001–1002.
[21] B. Fakhimi, D. Harrison, The voidage fraction near a horizontal tube immersed in a fluidised bed, Trans. Inst. Chem. Eng. 58 (2) (1980) 125–131.
[22] R. Chandran, Local heat transfer and fluidization dynamics around horizontal tubes in fluidized beds, Ph.D. Dissertation, Lehigh University, Bethlehem, PA, 1980.
[23] J.J. Ginoux, F.M. DeGeyter, B. Kilkis, Hydrodynamics of a two-dimensional fluidized bed in the vicinity of a cylinder with a horizontal axis, Catal. Rev. (1973) 274–282.